Direct observation of zonal dislocation in complex materials by atomic-resolution scanning transmission electron microscopy

AUTHOR(S):

Kishida, Kyosuke; Okutani, Masaomi; Inui, Haruyuki

Acta Materialia 228 (2022) 117756

Contents lists available at ScienceDirect

Acta Materialia

journal homepage: www.elsevier.com/locate/actamat

Direct observation of zonal dislocation in complex materials by atomic-resolution scanning transmission electron microscopy

Kyosuke Kishida[a,b,*], Masaomi Okutani[a], Haruyuki Inui[a,b]

[a] Department of Materials Science and Engineering, Kyoto University, Sakyo-ku, Kyoto 606-8501, Japan
[b] Center for Elements Strategy Initiative for Structural Materials (ESISM), Kyoto University, Sakyo-ku, Kyoto 606-8501, Japan

ARTICLE INFO

Article history:
Received 18 October 2021
Revised 18 January 2022
Accepted 12 February 2022
Available online 13 February 2022

Keywords:
Zonal dislocations
Sigma phase
Atomic shuffling
Micropillar compression

ABSTRACT

Dislocation glide to carry plastic deformation in simple metals and alloys is a well-understood process, but the process in materials with complex crystal structures is not yet understood completely as it can be very complicated often involving multiple atomic planes during dislocation glide. The zonal dislocation is one of the examples predicted to operate in complex materials, and during glide it involves multiple atomic planes called shear zone, in which non-uniform atom shuffling occurs. We report direct observation made by Z-contrast atomic-resolution microscopy of the zonal dislocation in the σ phase FeCr. The result confirms the zonal dislocation indeed operates in this material. Knowledge gained on the dislocation core structure will lead to improved understanding of deformation mechanisms in this and other complex crystal structures and provide ways to improve the brittleness of these complex materials.

1. Introduction

Plastic deformation of crystalline materials usually occurs by shear deformation (called slip) along a particular crystallographic direction (slip direction) on a particular crystallographic plane (slip plane) [1–3]. Such slip is usually carried by the glide motion of a lattice defect called 'dislocation', which is defined as the boundary (line defect) between slipped and unslipped regions on the slip plane [1–3]. 'Dislocation' is characterized by the line vector and the slip vector usually referred to as Burgers vector. The Burgers vector is in general the shortest translation vector and no crystalline defect is introduced before and after the passage of dislocation on the slip plane [1–3]. By definition, all atoms of one portion of a crystal above the slip plane are displaced with respect to another 'uniformly' by an amount determined by the Burgers vector upon the dislocation motion in the case of crystalline materials with a simple crystal structure such as face-centered cubic (FCC) and body-centered cubic (BCC) structures. However, when the crystal structure is complicated, the shearing process with these dislocations during slip can be more complex, involving a few to several successive atomic planes parallel to the slip plane, in contrast to dislocations in simple crystal structures, in which the shearing process involves only a single atomic plane [1–3].

One of the examples of such dislocations in complex materials is the 'synchroshear' dislocation that involves multiple (two, in many cases) successive parallel slip planes displaced synchronously along different (Burgers) vectors on each of planes so as to give the displacement corresponding to the sum of all the vectors as a whole. This concept was first predicted for basal slip in alumina by Kronberg [4], although it was recently claimed not to be the case in alumina (α-Al_2O_3) [5,6]. Later, however, the occurrence of synchroshear was indeed experimentally proved in transition-metal silicides with the C40 structure [7,8] and then for basal slip in Laves-phase compounds [9]. Another example is the 'zonal' dislocation that involves much more parallel slip planes as usually called 'shear zone', in which atoms in the zone slab move non-uniformly and cooperatively by varying amounts (as usually referred to as shuffling). The concept of zonal dislocation was first predicted also by Kronberg [10] for the {110}<001> slip in β-uranium with the tetragonal A_b structure [11,12], which is isostructural with the $D8_b$ structure (space group: $P4_2/mnm$ (No.136), Pearson symbol: $tP30$) of σ-FeCr [13]. The A_b structure of β-uranium and $D8_b$ structure of σ-FeCr are indeed isostructural with each other, since all five crystallographic sites, namely labelled as M(A) (Wyckoff position: 2*a*), M(B) (4*g*), M(C) (8*i*), M(D) (8*i*) and M(E) (8*j*), in σ-FeCr are of the mixed occupancy of Fe and Cr atoms [13, 14, Supplementary Fig. S1 and Table S1]. The unit cell of these two

* Corresponding author at: Department of Materials Science and Engineering, Kyoto University, Sakyo-ku, Kyoto 606-8501, Japan,
E-mail address: kishida.kyosuke.6w@kyoto-u.ac.jp (K. Kishida).

https://doi.org/10.1016/j.actamat.2022.117756

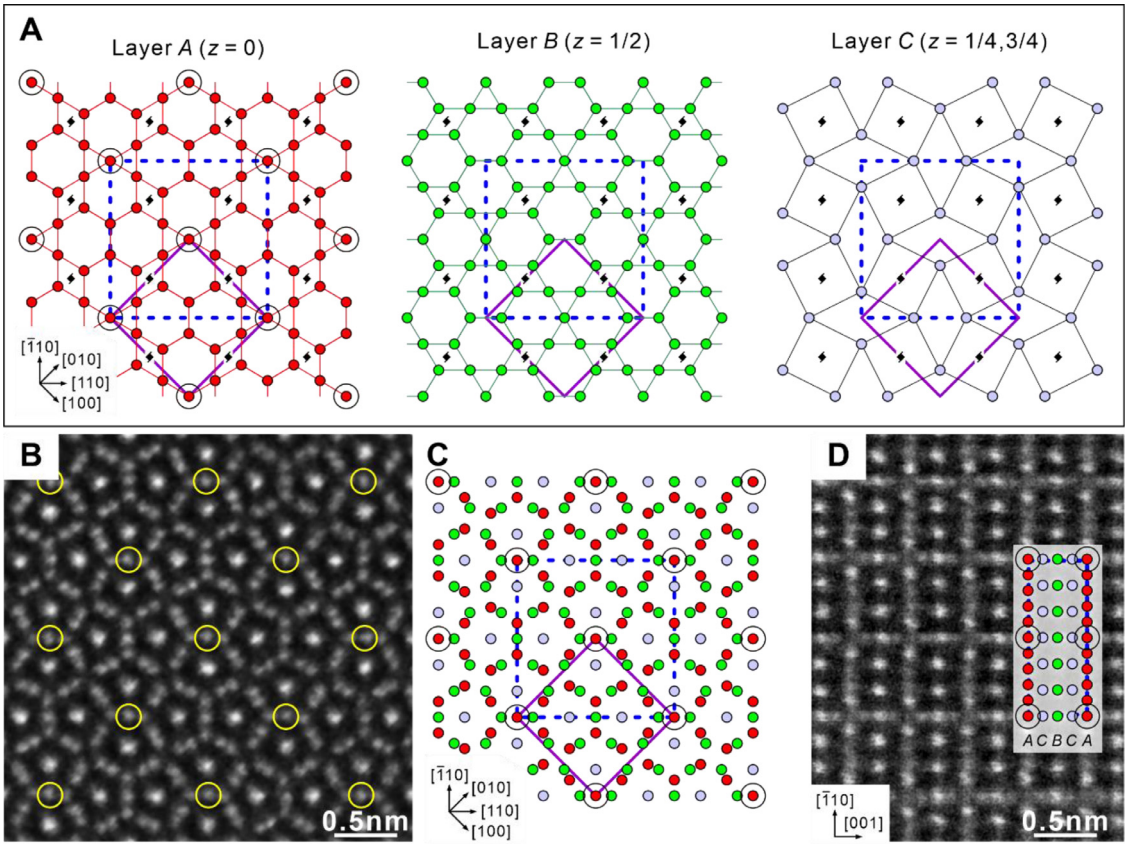

Fig. 1. (a) Atomic arrangements in three types of atomic layers of the tetragonal $A_b/D8_b$ structure. Open circles in layer *A* ($z = 0$) indicate the lattice points. Solid square and dashed square indicate the primitive and *C*-centered in-plane units, respectively. Black squares with two additional arms indicate 4_2 screw axes parallel to the *c*-axis. (b,d) Atomic resolution HAADF-STEM images of σ-FeCr projected along [001] and [110], and respectively. [001] and [110] projections of the $A_b/D8_b$ structure are indicated in (c) and as an insert of (d), respectively.

structures is composed of three different kinds of atomic layers designated as *A*, *B* and *C* stacked along the tetragonal *c*-axis with the stacking sequence of *ACBC* (Fig. 1(a)). Atomic layers *A* (at $z = 0$) and *B* (at $z = 1/2$), both of which are composed of atomic sites M(A), M(B), M(C) and M(D), have an identical atomic arrangement of the Kagome-type and they are related to each other by the 90°-rotation about the *c*-axis so as to generate 4_2 screw axes along the *c*-axis, which are indicated using black squares with two additional arms in Fig. 1(a). The atomic arrangement in Atomic layer *C* (at $z \sim 1/4$ and $3/4$[1]) being composed of M(E) sites only is described as corner-shared tilted-squares, where a four-fold axis is located at the center of each square. Fig. 1(b) and (d) are high-angle annular dark-field scanning transmission electron microscopy (HAADF-STEM) images together with schematic illustrations of atomic arrangements of σ-FeCr imaged along [001] and [110] (Fig. 1(c) and the inset of Fig. 1(d)), respectively. In the HAADF-STEM image projected along [110] (Fig. 1(d)), atomic columns in Atomic layers *A* and *B* are clearly imaged as bright spots while this is not the case for those in Atomic layer *C* because of the relatively low atomic density in Atomic layer *C*. Kronberg [10] considered that the shear along ⟨001⟩ on {110} should occur so as to avoid the encountering of Kagome-type Atomic layers *A* and *B* that are related to each other by the 90°-rotation at the slip plane during dislocation glide (Supplementary Fig. S2). He then predicted the slip occurs by the glide of dislocation that borders two atomic planes #1 and #2 separated by an interplanar distance of $2^{1/2}a/2$ (*a*: lattice constant), each of which contains 4_2 screw axes located at an interval of $2^{1/2}a/2$ (Fig. 2) [12]. The zone bordered by these two atomic planes are called 'shear zone', in which atoms in Atomic layers *A* and *B* are assumed to shuffle by a cooperative rotary-like motion of each of hexagonal Kagome-rings so that the atomic arrangement in Atomic layer *A* gradually turns into that of Atomic layer *B* and vice versa (i.e., 30°-rotation) within the shear zone as the dislocation passes through (Fig. 2). The dislocation was then named of the zonal-type [10]. However, it has never been experimentally verified to occur. This is because β-uranium is one of the typical radioisotopes, which prevents from further detailed experimental study of its dislocations. Another reason is that the brittleness of the sigma-phase (σ-FeCr, a famous embrittling phase in steel) arising from the complex crystal structure has made impossible for plastic flow to occur by dislocation glide (Supplementary Fig. S3).

However, micropillar compression testing has recently been proved to be a versatile tool to study fundamental deformation mechanisms of hard and brittle materials at temperatures well below the brittle-ductile transition temperature including room temperature [15–24]. Although the specimen size is small, the occurrence of plastic flow in brittle materials by micropillar compression testing has made possible to identify the opereative slip systems and analyze the dislocation fine structure with less ambiguity arising from dislocation climb often introduced during exposure at high temperature that is usually needed for plastic flow for bulk crystals. On top of that, single-crystal deforma-

[1] The atoms in Atomic layer *C* are slightly displaced from the ideal *z* of 1/4 and 3/4 so as to make the atomic layer slightly corrugated. However, such slight displacements are neglected throughout this paper for simplicity because they do not affect any of the following discussions.

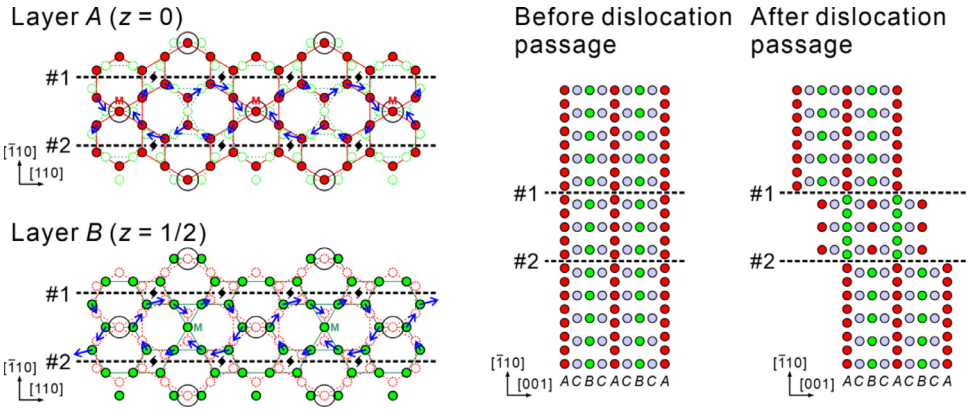

Fig. 2. Atomic shuffling models of a (110)[001] zonal dislocation proposed by Kronberg [10]. Blue arrows indicate the shuffling directions and magnitudes for atoms in layers A and B. Dashed lines #1-#2 indicate the pairs of glide planes defining the shear zones. Black squares with two additional arms indicate 4_2 screw axes parallel to the *c*-axis.

tion behaviors can easily be investigated even from bulk polycrystals by micropillar compression tesing, because of the small test specimen size. Here, we apply micropillar compression testing to room-temperature plastic deformation of the typical brittle material, sigma-phase compound (σ-FeCr) to confirm the activation of {110}<001> slip and then to investigate {110}<001> slip to see if the zonal dislocation is indeed responsible for the slip by atomic-resolution scanning transmission electron microscopy (STEM).

2. Experimental procedure

Ingots with a nominal composition of Fe-50 at.%Cr were prepared by Ar arc-melting of high-purity Fe (>99.99%) and Cr (>99.9%). The ingots were confirmed to crystallize into a homogeneous solid solution phase with the BCC structure. Specimens with approximate dimensions of 11 × 14 × 3.5 mm^3 cut from the ingot by spark machining were cold-rolled to 40% in thickness reduction. Then, the cold-rolled specimens encapsulated in quartz tube with Ar gas were annealed at 740 °C for 116 h, followed by air-cooling. The formation of the sigma-phase without any traces from other phases was confirmed by powder X-ray diffraction with a Rigaku MiniFlex II apparatus. The lattice parameters estimated by powder X-ray diffraction were $a = 0.8838$ nm and $c = 0.4569$ nm, both of which were a bit larger than those reported for FeCr with a composition of Fe-48 at.%Cr [14]. After mechanical polishing with diamond paste to mirror finish and analyzing crystallographic orientations of each grain by electron backscatter diffraction (EBSD) in a JEOL JSM-7001FA field-emission scanning electron microscope (FE-SEM), single-crystal micropillar specimens with square cross-sections having aspect ratios of 2~3:1 (height to edge length) were machined from a relatively large grain in the annealed specimen (average grain size of about 300 – 700 μm) with a JEOL JIB-4000 focused-ion beam (FIB) apparatus at an operating voltage of 30 kV. The edge lengths (L) of the square cross-sections ranged from 0.8 to 10.1 μm. A square cross-section was employed to facilitate the identification of slip planes and slip directions. The compression-axis orientation selected was [$\bar{5}$ 6 11] that is favorable for the operation of ($\bar{1}$10)[001] slip with the Schmid factor of 0.474.

Compression tests were conducted for micropillar specimens with a flat punch indenter tip on an Agilent Technologies Nano Indenter G200 nanomechanical tester at room temperature under the displacement-rate-controlled mode at a nominal strain rate of $1 \times 10^{-4}\ s^{-1}$. Slip planes were determined by slip trace analysis made on two orthogonal surfaces of the deformed micropillar specimen by scanning electron microscopy (SEM) with a JEOL JSM-7001FA electron microscope. Deformation microstructures developed in the deformed micropillars were investigated by transmission electron microscopy (TEM) and scanning transmission electron microscopy (STEM) with JEOL JEM-2000FX and JEM-ARM200F electron microscopes. Specimens for TEM/STEM observations were prepared by FIB-SEM in-situ lift-out technique using a FEI Quanta 3D 200i Dual-Beam system equipped with an Omniprobe nanomanipulator.

3. Results

Typical stress-strain curves and deformation microstructure of a micropillar specimen with the [$\bar{5}$ 6 11] loading-axis orientation are shown in Fig. 3. Plastic flow was observed to occur even at room temperature exhibiting a smooth transition from elastic to plastic deformation similarly to many ductile materials tested in the micropillar form (Fig. 3(a)). The yield stress defined as the elastic limit is very high exceeding 3 GPa without exhibiting a strong specimen size dependence. After compression, straight slip lines are clearly observed on the (35 $\overline{42}$ 39) side-surface, while slip lines on the (650) side-surface are observed only faintly (Fig. 3(b)). Slip trace analysis on the two orthogonal side surfaces confirms that slip occurs on (1$\bar{1}$0) and the slip direction is parallel to [001], which is contained in the (650) side-surface. The (1$\bar{1}$0)[001] slip system, which is one of the operative slip systems identified in the isostructural β-uranium, is successfully activated at room temperature in the [$\bar{5}$ 6 11]-oriented micropillar of the σ-FeCr. The critical resolved shear stress (CRSS) value calculated with the yield stress and the corresponding Schmid factor (0.474) for the (1$\bar{1}$0)[001] slip system is as high as 1.6 GPa. The very high CRSS value at room temperature is indicative of the inherent brittleness of σ-FeCr, as brittle failure usually occurs at a stress level well below such a high CRSS value in bulk crystals.

Deformation microstructures developed in the micropillar specimen deformed at room temperature was further investigated by STEM. The specimen for STEM observations was cut parallel to (110) by the in-situ lift-out technique so that the core structure of edge dislocations with the Burgers vector of [001] can be viewed end-on. Several traces of dislocation movement parallel to (1$\bar{1}$0) slip plane are observed to be always associated with surface steps (indicated by arrows in Fig. 3(c)), indicating that these traces are indeed introduced by dislocation glide at room temperature.

Fig. 4 shows a HAADF-STEM image of the core structure of a [001] dislocation with a pure edge character. Burgers circuit construction around the dislocation confirms that the Burgers vector

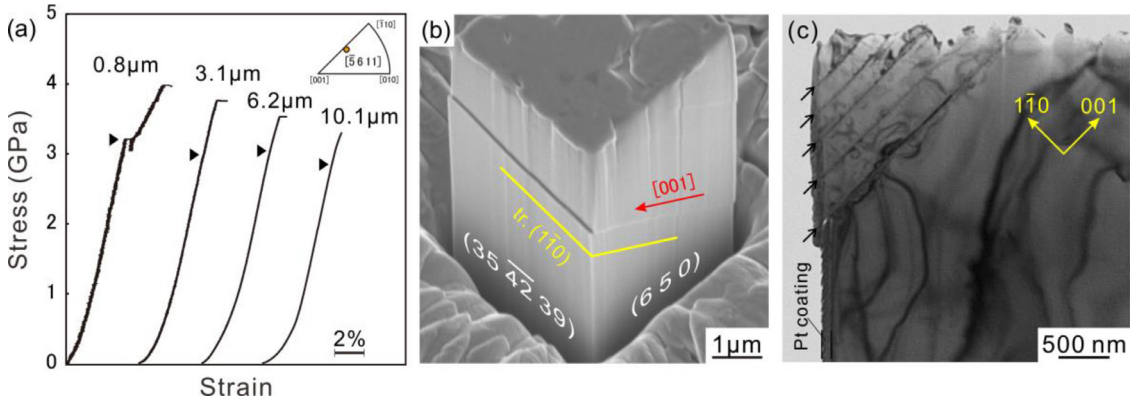

Fig. 3. (a) Typical stress-strain curves obtained for micropillar specimens of σ-FeCr single crystals with the loading axis of [$\bar{5}$ 6 11]. (b) A typical deformation microstructure of a micropillar specimen after compression. (c) A bright-field image of a deformed micropillar specimen of a [$\bar{5}$ 6 11]-oriented single crystal (L = 4.2 μm). Black arrows in (c) indicate where the surface steps are observed.

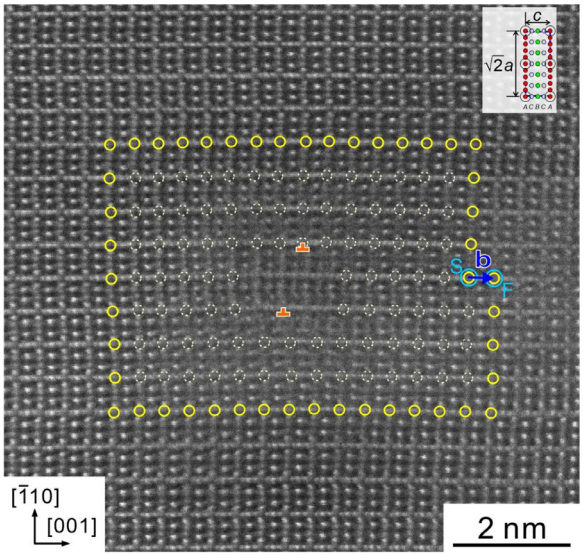

Fig. 4. Atomic resolution HAADF-STEM image of a core structure of a [001] dislocation introduced in a [$\bar{5}$ 6 11]-oriented micropillar specimen with L = 4.2 μm.

(**b**) of the dislocation is [001]. By locating the extra-half planes parallel to (001), two partial dislocations with an identical Burgers vector of **b** = 1/2[001] are clearly observed at positions marked by symbols ⊥ on two (110) planes separated by a distance corresponding to $2^{1/2}a$ (Fig. 4). The atomic arrangements on both left and right sides of these partial dislocations are identical to that of the perfect crystal, confirming that no stacking fault is formed on either side of each of the partial dislocations (see also Supplementary Fig. S4). These characteristics suggest that the observed [001] dislocation is of the zonal-type, as Kronberg [10] proposed. In Fig. 4, however, there are two points that are definitely inconsistent with what are expected from the Kronberg model for the zonal dislocation. Firstly, the thickness of the shear zone corresponding to the interplanar distance between two atomic planes on which the respective partial dislocations glide is twice as large as that assumed by Kronberg (Fig. 2). Secondly, the glide planes of these two partial dislocations are both located directly below the atoms on the lattice points (marked as planes #N1 and #N2 in Fig. 5), which are totally different from those proposed by Kronberg (marked as planes #1 and #2 in Fig. 2). These observations clearly indicates that the dislocation responsible for {110}<001> slip in σ-FeCr is indeed ⟨001⟩ dislocations of the zonal-type but that the atomic shuffle occurring in the shear zone for the zonal dislocation is different from what is predicted for the same [001] dislocation by Kronberg [10].

4. Discussion

Here, we discuss possible atomic shuffling in the shear zone of the zonal dislocation. In the Kronberg model, atoms in Atomic layers *A* and *B* are considered to shuffle by a cooperative rotary-like movement so that the atomic arrangement in Atomic layer *A* gradually turns into that of Atomic layer *B* and vice versa within the shear zone [10], as shown in Fig. 2. Of importance to notice in this model is that while rotary-like atomic shuffling for most atoms occurs within each of (001) Kagome atomic layers, the atoms labelled M in Fig. 2 are assumed to move in the direction perpendicular to the (001) Kagome atomic plane, pass through an intermediate layer *C* and finally penetrate into the next Kagome layer so as to occupy a missing site in the next Kagome layer after the rotary-like shuffling movement. However, we here propose an alternative model in which rotary-like atomic shuffling for all atoms occurs within each of (001) Kagome atomic layers (Fig. 5), based on the atomic-resolution STEM observation of Fig. 4. Blue arrows in Fig. 5 indicate the direction and magnitude of the proposed atomic shuffling movement. The (001) Kagome atomic layers in the shear zone are indexed in Fig. 6(a) with Kronberg's original notation in [10]. Atomic layers *C* are not illustrated in Fig. 6(a), since they are not involved with atomic shuffling. Atomic layers with odd and even indices are those originally with the atomic arrangements of layers *A* and *B*, respectively. Details of atomic shuffling that occurs for each of (001) Kagome atomic layers indexed in Fig. 6(a) are shown in Fig. 6(b). Atomic layers 3z and 4z in Fig. 6(b) possess the original Kagome-type atomic arrangement of layers *A* and *B*, respectively. Atomic layers indexed through 5z to 10z in Fig. 6(b) have transitional atomic arrangements from the layer-*A* type to layer-*B* type and vice versa. These transitional atomic arrangements shown in Fig. 6(b) were obtained simply assuming that the atom movements occur along the blue vectors in Fig. 5. In these atomic planes of 5z to 10z, all atoms are shuffled from their original positions within each of the atomic planes and consequently, the alignment of atoms along the [110] direction (the horizontal direction in Fig. 6(b)) in each of (001) Kagome atomic layers, which is normally observed in the crystal structure, is disturbed in these atomic planes with transitional atomic arrangements. Such atomic shuffling in the shear zone (i.e., loss of atom alignment along the [110] direction) would result in the intensity elongation and reduction of bright spots corresponding to the

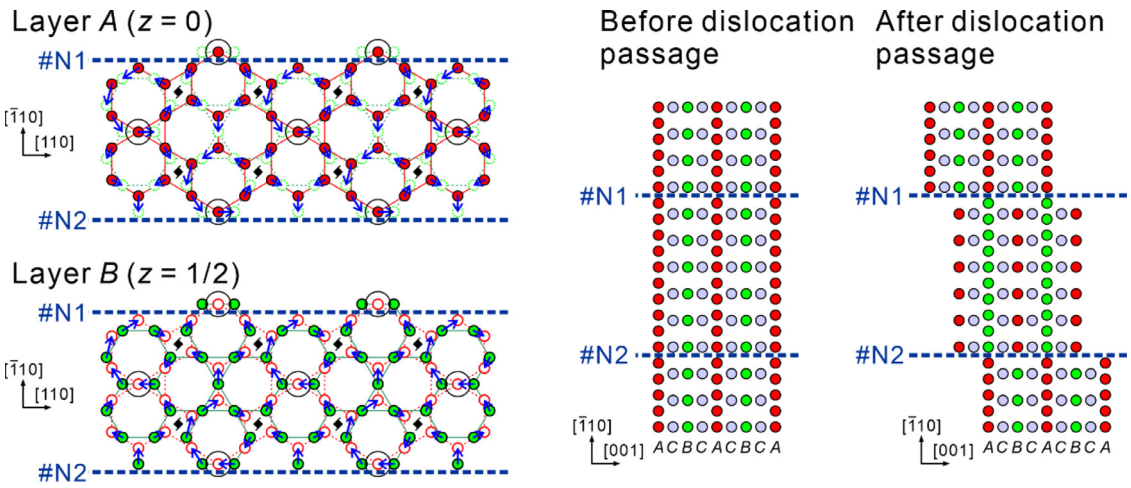

Fig. 5. New atomic shuffling model of a (110)[001] zonal dislocation proposed in this study. Blue arrows indicate the shuffling directions and magnitudes for atoms in layers *A* and *B*. Dashed lines #N1-#N2 indicate the pairs of glide planes defining the shear zones. Black squares with two additional arms indicate 4_2 screw axes parallel to the *c*-axis.

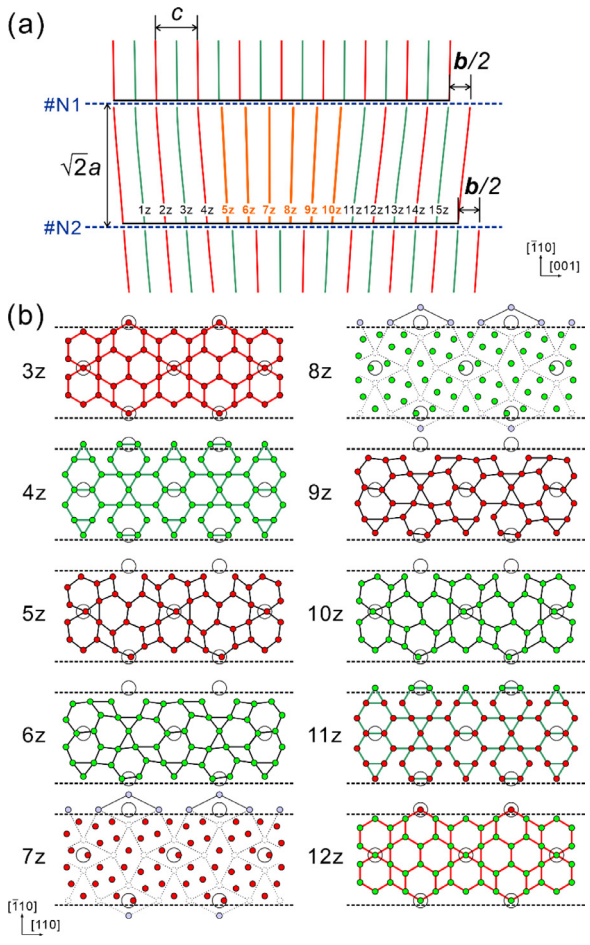

Fig. 6. (a) Schematic illustration showing the displacements of the (001) atomic layers in the vicinity of a zonal dislocation core in the shear zone. Plane indices 1z to 15z are used after the model proposed by Kronberg [10]. (b) Approximate atomic arrangement in (001) atomic layers 3z-12z in the vicinity of the edge dislocation core in the shear zone. Red, Green and cyan circles indicate atoms that are originally in layers *A*, *B* and *C*, respectively. Dashed lines indicate the glide planes (#N1 and #N2 in Fig. 5) defining the shear zone. Projected positions of lattice points are indicated with open circles as a guide.

[110] atomic rows in the (001) Kagome atomic layers with transitional atomic arrangements, as indeed experimentally observed by atomic-resolution STEM imaging with the [110] incidence (Fig. 4).

After the complete passage of one zonal dislocation, the atomic arrangements of layers 11z and 12z in Fig. 6(b), which originally had those of the layer-*A* and layer-*B* type, turn into those of the layer-*B* and layer-*A* types, respectively. In the present model, all atomic shuffling in the shear zone occurs within each of (001) Kagome atomic layers, and hence, the present model is simpler and more convincing than the original Kronberg model that requires complex atomic shuffles for some atoms along the direction perpendicular to the (001) atomic layers. The doubled thickness of the shear zone as well as the exact location of the glide planes for the two partial dislocations directly below the atoms on the lattice points enables simpler and more convincing atomic shuffling in the shear zone of the zonal dislocation. The present model of the zonal dislocation can be extended to other materials with complex crystal structures that consist of stacked Kagome atomic layers.

The atomic arrangement of the core of the zonal dislocation responsible for {110}<001> slip in the sigma-phase compound FeCr isostructural with β-uranium was directly observed for the first time by atomic-resolution STEM and the model for atomic shuffling in the shear zone of the zonal dislocation, which is consistent with the observed STEM image, was successfully established. Further understanding could be gained from first-principles calculation for the shuffling process in the shear zone during the motion of the zonal dislocation. Understanding of the dislocation core structure and its influence on the dislocation mobility is central to improvement of the low-temperature mechanical properties of otherwise brittle materials. Since the motion of the zonal dislocations requires atomic shuffling in the shear zone, the stress needed to move these dislocations is expected to be reduced at high temperatures where atomic shuffling is aided by thermal activation, thereby promoting dislocation motion and mitigating the brittleness. This is consistent with many experimental observations that heat-resistant austenitic and duplex steels are not embrittled by precipitation of the sigma-phase compound at the service temperature [25–28]. One way to avoid the brittleness of the sigma-phase compound at low temperature is utilizing the size effect, as in the present study, in which the sigma-phase compound FeCr exhibits deformability at room temperature as the specimen size is reduced to the micron-meter order. Okada et al. [29] indeed reported that

the sigma-phase compound with a basic composition of FeMo contributes to strengthening of maraging steel during aging up to the peak strength without deteriorating the ductility when the sigma-phase compound FeMo is fine and precipitated homogeneously in the matrix. From the atomic arrangement of the zonal dislocation core, how easily the atomic shuffling in the shear zone occurs seems to play an essential role in determining the ease of the dislocation motion. The atomic shuffling involves a cooperative rotary-like movement of atoms in each of (001) Kagome layers. In view of the fact that such rotary-like atom movement in the (001) Kagome layers occurs with an atom in the atomic layer C of corner-shared tilted square as the rotation center (8*j* sites in the Wycoff notation), the atomic shuffling thereby the dislocation motion is expected to occur more easily if, for example, an alloying element that preferentially occupies the 8*j* sites enlarging the *a*-axis dimension is added. Interestingly, Mo is expected to behave in that way when judged from the lattice constants and the Mo preference in the M(E) (8*j*) sites of Fe/Mo mixed occupancy [13,30]. A nano-indentation study to verify that the hardness decreases when some of Cr in FeCr is replaced by Mo is currently under survey in our laboratory.

5. Conclusions

(1) The atomic arrangement of the core of the ⟨001⟩ zonal dislocation in the sigma-phase compound FeCr is directly observed for the first time by atomic-resolution STEM and the model for atomic shuffling in the shear zone of the zonal dislocation is successfully established.
(2) Unlike in the original Kronberg model that requires complex atomic shuffles for some atoms along the direction perpendicular to the (001) atomic layers, all atomic shuffling in the shear zone in the present model occurs simply within each of (001) Kagome atomic layers. The difference between the two models comes from the thickness of the shear zone. The doubled thickness of the shear zone as well as the exact location of the glide planes for the two partial dislocations directly below the atoms on the lattice points in the present model enables simpler and more convincing atomic shuffling in the shear done of the zonal dislocation.
(3) From the atomic arrangement of the zonal dislocation core, the motion of the zonal dislocations thereby the brittleness of the compound is expected to be controlled by the ease of the atomic shuffling in the shear zone. Some strategy to avoid the brittleness is discussed in terms of how a cooperative rotary-like movement of atoms in each of (001) Kagome layers is made to occur more easily.

Declaration of Competing Interest

The authors declare that they have no known competing financial interests or personal relationships that could have appeared to influence the work reported in this paper.

Acknowledgements

This work was supported by JSPS KAKENHI grant numbers JP18H01735, JP18H05478, JP18H05450, JP18H05451, JP19H00824, JP19K22053, JP20K21084, JP21H01651 and the Elements Strategy Initiative for Structural Materials (ESISM) of MEXT (Grant number JPMXP0112101000), and in part by JST-ALCA (Grant Number JPMJAL1004) and JST CREST (Grant number JPMJCR1994).

Supplementary materials

Supplementary material associated with this article can be found, in the online version, at doi:10.1016/j.actamat.2022.117756.

References

[1] J. Friedel, Dislocations, Adison-Wesley Publ. Co., Reading, MA, 1964.
[2] R.W.K. Honeycombe, The Plastic Deformation of Metals, Edward Arnold (Publ.) ltd., London, 1968.
[3] P.M. Anderson, J.P. Hirth, J. Lothe, Theory of Dislocations, 3rd. ed., Cambridge Univ. Press, Cambridge, 2017.
[4] M.L. Kronberg, Plastic deformation of single crystals of sapphire: basal slip and twinning, Acta Metall. 5 (1957) 507–524.
[5] J.B. Bilde-Sørensen, B.F. Lawlor, T. Geipel, P. Pirouz, A.H. Heuer, K.P.D. Lagerlöf, On basal slip and basal twinning in sapphire (α-Al_2O_3) – I. Basal slip revisited, Acta Metall. 44 (1996) 2145–2152.
[6] A.H. Heuer, C.L. Jia, K.P.D. Lagerlöf, The core structure of basal dislocations in deformed sapphire (α-Al_2O_3), Science 330 (2010) 1227–1231.
[7] H. Inui, M. Moriwaki, S. Ando, M. Yamaguchi, Plastic deformation of single crystals of $CrSi_2$ with the C40 structure, Mater. Sci. Eng. A239-240 (1997) 63–68.
[8] H. Inui, M. Moriwaki, K. Ito, M. Yamaguchi, Plastic deformation of single crystals of $Mo(Si,Al)_2$ with the C40 structure, Philos. Mag. A 77 (1998) 375–394.
[9] M.F. Chisholm, S. Kumar, P. Hazzledine, Dislocations in complex materials, Science 307 (2005) 701–703.
[10] M.L. Kronberg, Atom movements and dislocation structures for plastic slip in single crystals of β-uranium, J. Nucl. Mater 1 (1959) 85–95.
[11] A.N. Holden, Growth and crystallography of deformation of β-phase Uranium single crystals, Acta Cryst 5 (1952) 182–184.
[12] A.C. Lawson, C.E. Olsen, J.W. Richardson Jr., M.H. Mueller, G.H. Lander, Structure of β-uranium, Acta Cryst B44 (1988) 89–96.
[13] G. Bergman, D.P. Shoemaker, The determination of the crystal structure of the σ phase in iron-chromium and iron-molybdenum systems, Acta Cryst 7 (1954) 857–865.
[14] H.L. Yakel, Atom distributions in sigma phases. I. Fe and Cr atom distributions in a binary sigma phase equilibrated at 1063, 1013 and 923K, Acta Cryst B39 (1983) 20–28.
[15] M.D. Uchic, D.M. Dimiduk, J.N. Florando, W.D. Nix, Sample dimensions influence strength and crystal plasticity, Science 305 (2004) 986–989.
[16] M.D. Uchic, P.A. Shade, D.M. Dimiduk, Plasticity of micrometer-scale single crystals in compression, Annu. Rev. Mater. Res. 39 (2009) 161–186.
[17] J. Michler, K. Wasmer, S. Meier, F. Östlund, K. Leifer, Plastic deformation of gallium arsenide micropillars under uniaxial compression at room temperature, Appl. Phys. Lett. 90 (2007) 043123.
[18] S. Korte, W.J. Clegg, Discussion of the dependence of the effect of size on the yield stress in hard materials studied by microcompression of MgO, Philos. Mag. 91 (2011) 1150–1162.
[19] S. Korte-Kerzel, Microcompression of brittle and anisotropic crystals: recent advances and current challenges in studying plasticity in hard materials, MRS Comm 7 (2017) 109–120.
[20] S. Schröders, S. Sandlöbes, C. Birke, M. Loeck, L. Peters, C. Tromas, S. Korte-Kerzel, Room temperature deformation in Fe_7Mo_6 μ-phase, Int. J. Plasticity 108 (2018) 125–143.
[21] K. Kishida, T. Maruyama, H. Matsunoshita, T. Fukuyama, H. Inui, Micropillar compression deformation of single crystals of Mo_5SiB_2 with the tetragonal $D8_l$ structure, Acta Mater. 159 (2018) 416–428.
[22] K. Kishida, Y. Shinkai, H. Inui, Room temperature deformation of 6H-SiC single crystals investigated by micropillar compression, Acta Mater. 187 (2020) 19–28.
[23] K. Kishida, T. Fukuyama, T. Maruyama, Room temperature deformation of single crystals of Ti_5Si_3 with the hexagonal $D8_8$ structure investigated by micropillar compression tests, Sci. Rep. 10 (2020) 17983.
[24] K. Kishida, T. Maruyama, T. Fukuyama, H. Inui, Micropillar compression deformation of single crystals of α-Nb_5Si_3 with the tetragonal $D8_l$ structure, Sci. Tech. Adv. Mater 21 (2020) 805–816.
[25] E.E. Levin, E.M. Pivnik, P.M. Libman, The effect of sigma phase on the mechanical properties of heat resistant steels, Met. Sci. Heat Treat. Met. 1 (1959) 19–21.
[26] Y. Maehara, Superplastic deformation mechanism of δ/γ duplex stainless steels, Trans. ISIJ 27 (1987) 705–712.
[27] Y.S. Han, S.H. Hong, The effects of thermo-mechanical treatments on superplasticitry of Fe-24Cr-7Ni-3Mo-0.14N duplex stainless steel, Scripta Mater 36 (1997) 557–563.
[28] C.H. Shek, K.W. Wong, J.K.L. Lai, D.J. Li, Hot tensile properties of 25Cr-8Ni duplex stainless steel containing cellular ($\sigma + \gamma_2$) structure after various thermal treatments, Mater. Sci. Eng A266 (1999) 30–61.
[29] Y. Okada, Application of intermetallic compound precipitates for iron and steel, Bull. Japan Inst. Met. 28 (1989) 589–594.
[30] C.G. Wilson, F.J. Spooner, Ordering of atoms in the sigma phase FeMo, Acta Cryst 16 (1963) 230–231.